Diagnosing the sensitivity of particulate nitrate to precursor emissions using satellite observations of ammonia and nitrogen dioxide

Ruijun Dang[1], Daniel J. Jacob[1], Shixian Zhai[2], Pierre Coheur[3], Lieven Clarisse[3], Martin Van Damme[3,4], Drew C. Pendergrass[1], Jin-soo Choi[5], Jin-soo Park[5], Zirui Liu[6], and Hong Liao[7]

[1] John A. Paulson School of Engineering and Applied Sciences, Harvard University, Cambridge, MA 02138, USA.

[2] Earth System Science Programme, State Key Laboratory of Agrobiotechnology, and Institute of Environment, Energy and Sustainability, The Chinese University of Hong Kong, Sha Tin, Hong Kong.

[3] Université libre de Bruxelles (ULB), Spectroscopy, Quantum Chemistry and Atmospheric Remote Sensing (SQUARES), Brussels, Belgium.

[4] Royal Belgian Institute for Space Aeronomy (BIRA-IASB), Brussels, Belgium.

[5] Air Quality Research Division, National Institute of Environmental Research, Incheon 22689, South Korea.

[6] State Key Laboratory of Atmospheric Boundary Layer Physics and Atmospheric Chemistry, Institute of Atmospheric Physics, Chinese Academy of Sciences, Beijing, China.

[7] Jiangsu Key Laboratory of Atmospheric Environment Monitoring and Pollution Control, Collaborative Innovation Center of Atmospheric Environment and Equipment Technology, School of Environmental Science and Engineering, Nanjing University of Information Science and Technology, Nanjing 210044, China.

Correspondence to: Ruijun Dang (rjdang@g.harvard.edu)

Key Points:

- Reducing particulate nitrate pollution requires understanding its local sensitivities to NH_3, NO_x, and VOC emissions.
- Satellite observation of the NH_3/NO_2 column ratio is an effective indicator for diagnosing these sensitivities.
- IASI NH_3 and OMI NO_2 observations reveal varying regimes of nitrate sensitivity across wintertime East Asia.

Abstract

Particulate nitrate is a major component of fine particulate matter ($PM_{2.5}$), and its formation may be varyingly sensitive to emissions of ammonia (NH_3), nitrogen oxides ($NO_x \equiv NO + NO_2$), and volatile organic compounds (VOCs), depending on local conditions. Diagnosing the dominant sensitivities is critical for successful air quality management. Here, we show that satellite measurements of tropospheric NH_3 and NO_2 columns can be used to diagnose the dominant sensitivity regime through the NH_3/NO_2 column ratio as indicator together with the NO_2 column. We demonstrate the effectiveness of this indicator with the GEOS-Chem atmospheric chemistry model and define thresholds to separate the different sensitivity regimes. Applying the method to wintertime IASI and OMI observations in East Asia reveals that surface nitrate is dominantly VOC-sensitive in the southern North China Plain (NCP), NO_x-sensitive in most of the East China Plain, and NH_3-sensitive in the northern NCP, southern China, and Korea.

Plain Language Summary

We present a novel application of satellite remote sensing to better understand the causes of particulate nitrate pollution. Particulate nitrate is a major air pollutant throughout the urbanized world. It is produced by atmospheric oxidation of emitted nitrogen oxides (NO_x) but may be more sensitive to emissions of ammonia (NH_3) or volatile organic compounds (VOCs). Understanding which of NH_3, NO_x, or VOC emissions is most important in driving nitrate formation is critical for air quality management. We show that satellite measurements of the NH_3/NO_2 column ratio along with NO_2 columns is an effective indicator to determine the dominant sensitivity regime (NH_3-, NO_x-, or VOC-sensitive). We develop this approach using an atmospheric chemistry model and apply it to wintertime satellite observations in East Asia. The approach should be applicable to other continents, seasons, and a broader range of satellite instruments, providing valuable insights for particulate nitrate reduction strategies.

1. Introduction

Particulate nitrate (pNO_3^-) is a major component of fine particulate matter ($PM_{2.5}$) throughout the urbanized world and particularly in winter. It drives $PM_{2.5}$ pollution events in East Asia (Li et al., 2018; Tian et al., 2019; Q. Xu et al., 2019; H. Kim et al., 2020; Kim et al., 2022), North America (Franchin et al., 2018; Womack et al., 2019), and Europe (Bressi et al., 2021). Other $PM_{2.5}$ components in East Asia have decreased rapidly over the past decade in response to emission controls (Zhai et al., 2019), but pNO_3^- has not (Li et al., 2019; Leung et al., 2020; Zhou et al., 2022; Zhai et al., 2023). In eastern China, wintertime pNO_3^- concentrations have been flat over the past decade despite a 30% decrease in NO_x emissions (Fu et al., 2020; Chuang et al., 2021; Zhai et al., 2021). pNO_3^- has become a key target for further improving $PM_{2.5}$ air quality but the means to achieve this are not clear.

pNO_3^- is produced by the oxidation of nitrogen oxide radicals ($NO_x \equiv NO + NO_2$) to nitric acid (HNO_3). HNO_3 condenses into the aerosol in the presence of alkalinity, mostly from ammonia (NH_3) available after sulfate neutralization (Guo et al., 2018). The resulting pNO_3^- is mainly in the fine $PM_{2.5}$ aerosol mode. NO_x in urban areas mainly comes from fuel combustion. NH_3 originates from agricultural activities including fertilizer use and livestock manure, but vehicle emissions could also be important in urban areas (Farren et al., 2020; Y. Wang et al., 2023). Oxidation of NO_x to HNO_3 is by the hydroxyl radical (OH) during the daytime and by ozone (O_3) at night, both of which depend on the levels of NO_x and volatile organic compounds (VOCs). VOCs originate from combustion, industry, vegetation, and open fires (Shen et al., 2019).

pNO_3^- concentrations are generally highest in winter when low temperatures favor partitioning into the aerosol. Formation of pNO_3^- may then be dominantly sensitive to the gas in shortest supply, either NH_3 or HNO_3 (Nenes et al., 2020), while the NO_x to HNO_3 conversion is limited by either the abundance of NO_x or VOCs (Kleinman, 1994; Womack et al., 2019). Other factors can further complicate these relationships of pNO_3^- to emitted precursors, including competing deposition between HNO_3 and pNO_3^- (Zhai et al., 2021), other sources of aerosol alkalinity (Guo et al., 2018), and NO_x oxidation to organic nitrates (Romer Present et al., 2020). Coarse pNO_3^- can also form from uptake of HNO_3 by alkaline soil dust and sea salt in dusty and coastal areas (Zhai et al., 2023). The sensitivity of pNO_3^- concentrations to NH_3, NO_x, and VOC emissions is thus nonlinear and complex, requiring different control strategies under different conditions.

Here we present a new satellite-based method to diagnose locally the sensitivities of fine pNO_3^- formation to NH_3, NO_x, and VOC emissions. We use for this purpose satellite measurements of the tropospheric column concentrations of NH_3 (Ω_{NH3}) and NO_2 (Ω_{NO2}). NH_3 measurements from space have been available from the IASI instrument since 2007 (Clarisse et al., 2009), and from the CrIS instrument since 2012 (Shephard and Cady-Pereira, 2015). NO_2 measurements from space began with the GOME instrument in 1995 (Martin et al., 2002) and have continued with the OMI instrument since 2005 (Lamsal et al., 2021), the TROPOMI instrument since 2017 (van Geffen et al., 2020), and the GEMS geostationary instrument since 2020 (J. Kim et al., 2020). We demonstrate the method for East Asia in winter, using observations from OMI and IASI. Our approach draws similarity to the common use of the space-based formaldehyde $HCHO/NO_2$ ratio as an indicator for whether O_3 formation is NO_x- or VOC-limited (Martin et al., 2004; Duncan et al., 2010; Jin et al., 2020).

2. Theoretical basis: Ω_{NH3} and Ω_{NO2} as indicators of nitrate formation regime

The main pathway for fine pNO_3^- formation is the joint condensation of NH_3 and HNO_3, governed by a thermodynamic equilibrium constant K dependent on temperature and relative humidity (RH) (Stelson and Seinfeld, 1982):

$$K = p_{NH_3} \times p_{HNO_3} \quad (1),$$

where p is partial pressure. At low wintertime temperatures and/or high RH, the low value of K leads to titration where pNO_3^- formation is mainly sensitive to the gas in shortest supply, either NH_3 or HNO_3. At warmer temperatures, NH_3 and HNO_3 may coexist in the gas phase but the dominant sensitivity is still to the gas in shortest supply (Nenes et al., 2020). Scavenging of NH_3 by acid sulfate may totally suppress pNO_3^- formation when sulfate is in excess of NH_3 (Ansari and Pandis, 1998). Dust and sea salt particles can also drive HNO_3 into the aerosol through added alkalinity or chloride displacement (Alexander et al., 2005; Fairlie et al., 2010), though this tends to be in coarser particles than $PM_{2.5}$. Henceforth we will refer to pNO_3^- as the fine $PM_{2.5}$ component of nitrate.

The dominant sensitivities for pNO_3^- formation can be determined in field campaigns by measuring the molar ratio R of free ammonia after sulfate neutralization ($NH_3 + NH_4^+ - 2\times SO_4^{2-}$) to total nitrate ($NO_3^T \equiv HNO_3 + pNO_3^-$) (Petetin et al., 2016; Z. Xu et al., 2019). $R > 1$ indicates dominant sensitivity to HNO_3, while $R < 1$ indicates dominant sensitivity to NH_3. The gas-phase NH_3/HNO_3 ratio can also serve as an indicator but its threshold for transition between regimes may depart from unity when NO_3^T is heavily partitioned into the aerosol and the resulting HNO_3 concentration is very low. A dominant sensitivity to HNO_3 would be expected to translate into a dominant sensitivity to NO_x emissions, but the conversion of NO_x to HNO_3 may in fact be limited by the supply of VOCs under VOC-limited conditions for oxidant (OH and O_3) formation. Womack et al. (2019) point out that this may cause pNO_3^- formation to be most sensitive to VOC emissions under strongly VOC-limited conditions as frequently occur in urban environments in winter.

Satellites measure tropospheric columns of NH_3 (Ω_{NH3}) and NO_2 (Ω_{NO2}). It follows from the above discussion that the measured $\Omega_{NH3}/\Omega_{NO2}$ ratio should give an indicator of the sensitivity of pNO_3^- formation to precursor emissions, in a manner useful to air quality management. Application of this indicator may be complicated by the vertical gradients of NH_3 and NO_2 concentrations, by the presence of sulfate, and by the limiting regime for oxidation of NO_x to HNO_3. A model analysis can evaluate these complications, and this is discussed in the next section. Satellite observations of HCHO columns (Ω_{HCHO}) could in principle distinguish between NO_x- and VOC-limited oxidant regimes through consideration of the $\Omega_{HCHO}/\Omega_{NO2}$ ratio, but in practice wintertime Ω_{HCHO} concentrations are near or below the detection limit (Zhu et al., 2014; Zhu et al., 2017). Very high Ω_{NO2} values can be used instead as an indicator of VOC-limited conditions (Sillman, 1995).

3. Evaluation in the GEOS-Chem model environment

To analyze the value of the $\Omega_{NH3}/\Omega_{NO2}$ ratio as an indicator for the sensitivity of pNO_3^- formation to emissions, we conduct sensitivity simulations with the GEOS-Chem global atmospheric chemistry model. We use GEOS-Chem version 13.4.1 (DOI: https://zenodo.org/record/6564702) with options and modifications described below. The simulations are driven by MERRA-2 meteorology and are conducted at a nested resolution of 0.5° × 0.625° for East Asia (90°-145°E,

10°-55°N) over the 1-31 January 2017 period, with boundary conditions updated every 3 h from a 4° × 5° global simulation. The simulation is spun up for 6 months for initialization.

GEOS-Chem includes detailed oxidant-aerosol chemistry (Wang et al., 2021).Thermodynamic pNO_3^- formation from NH_3-HNO_3-H_2SO_4-HCl mixtures is calculated by ISORROPIA II (Fountoukis and Nenes, 2007) and defines in the model the $PM_{2.5}$ component of pNO_3^-. The model also includes uptake of HNO_3 by coarse sea salt aerosol (Wang et al., 2021) but this does not contribute to $PM_{2.5}$ and is not considered here in pNO_3^- accounting. Uptake of HNO_3 by dust is included in GEOS-Chem as an option (Fairlie et al., 2010; Zhai et al., 2023) but is not used in our simulation. We use the wet deposition scheme of Luo et al. (2020) , which is an option in GEOS-Chem and has proven to be important for successful simulation of pNO_3^- (Luo et al., 2019; Luo et al., 2020; Zhai et al., 2021). We also add to our simulation the photolysis of aerosol nitrate, which improves the simulation of tropospheric NO_2 column observations in GEOS-Chem though the effect is small in winter (Dang et al., 2023; Shah et al., 2023). Global anthropogenic emissions are from the Community Emissions Data System (CEDS) (McDuffie et al., 2020) superseded by the MEIC inventory for China (Zheng et al., 2018) and the KORUSv5 inventory for South Korea. Other emissions settings are as described in Dang et al. (2023).

Figure 1 compares simulated pNO_3^- concentrations from our simulation with measurements from observational networks and field studies in China and Korea in winter 2016-2017. Table S1 gives site details. Most observations are centered on January 2017, but some are for December 2016, and some are for the whole winter (DJF). All are compared to GEOS-Chem in January 2017. We find that GEOS-Chem can well simulate the ensemble observations with a correlation coefficient $r = 0.82$, a reduced-major-axis (RMA) regression slope of 0.98 ± 0.15, and a normalized mean bias (NMB) of 9%. There is one site in Xi'an where observed pNO_3^- is anomalously high (averaging 36 μg m^{-3}) and this is not captured by the model. This site is excluded from the regression analysis above. Overall, the successful simulation lends confidence in using the model to study the sensitivity of pNO_3^- to precursor emissions.

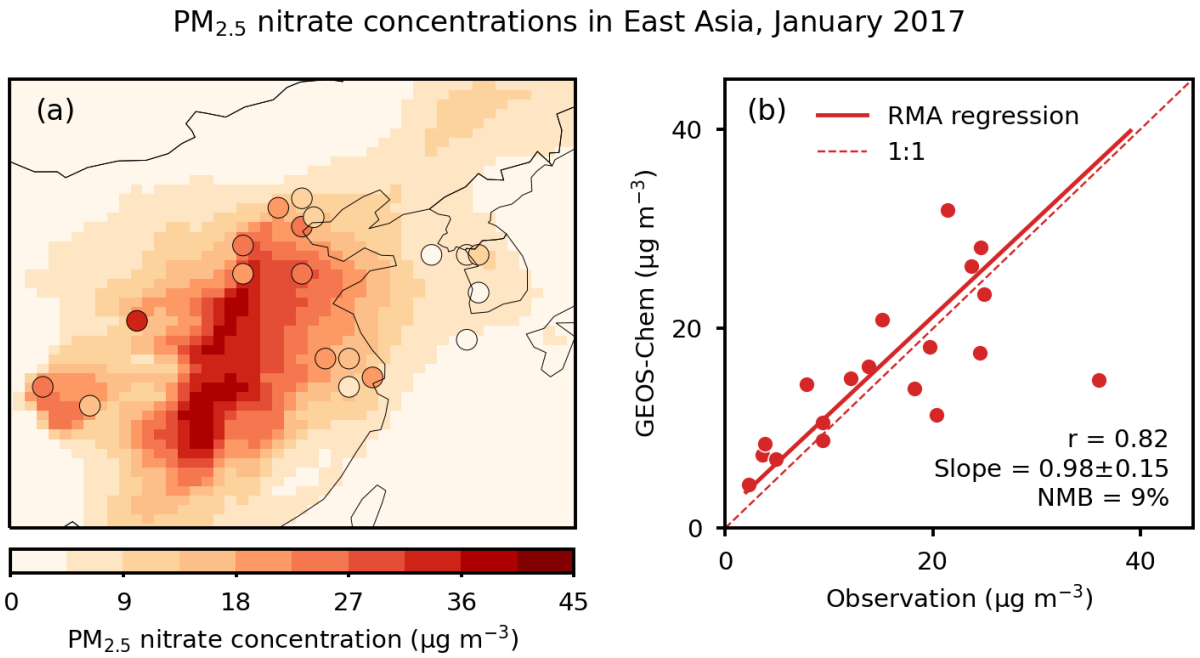

Figure 1. Surface $PM_{2.5}$ nitrate concentrations in China and Korea. Mean GEOS-Chem model concentrations for January 2017 are compared to observations at a number of sites (Table S1) over December-February 2017, averaged over the observing periods. Panel (a) shows the spatial distribution, with observations as circles and GEOS-Chem as solid contours. Panel (b) shows the correlation between model and observations at individual sites including correlation coefficient (r), normalized mean bias (NMB), reduced-major-axis (RMA) regression line and slope (± 95% confidence interval), and 1:1 dashed line. The RMA regression excludes the Xi'an site where observed pNO_3^- is anomalously high. Site details are in Table S1.

We diagnose the local pNO_3^- sensitivity to NH_3, NO_x, and VOC emissions in the model by conducting sensitivity simulations with individual emissions reduced by 20%. The reduction is applied to all sources (anthropogenic and natural) but the sources in winter are mainly anthropogenic. The local model sensitivity S_i of pNO_3^- to emissions E_i of species i for individual $0.5^o \times 0.625^o$ grid cells is calculated from the relative model differences (Δ) between the sensitivity and base simulations as:

$$S_i = \frac{\Delta \log[pNO_3^-]}{\Delta \log E_i} \qquad (2),$$

where i refers to NH_3, NO_x, or VOC, and $[pNO_3^-]$ refers to 24-h average monthly mean concentrations in surface air. A sensitivity $S_i = 1$ indicates that a 20% reduction in emissions of precursor i results in a corresponding 20% decrease in surface pNO_3^- concentrations. By comparing S_{NH3}, S_{NOx}, and $S_{VOC,}$ we can determine whether pNO_3^- in a model grid cell is most NH_3-, NO_x-, or VOC-sensitive.

Figure 2 shows the model relationship between the dominant pNO_3^- sensitivity and the observable surface and satellite indicators discussed in Section 2. Individual circles show the dominant sensitivities S_i for monthly mean surface pNO_3^- concentrations in individual grid cells. We use the NH_3/HNO_3 gas-phase molar ratio as surface indicator instead of R because it is better connected to the $\Omega_{NH3}/\Omega_{NO2}$ satellite indicator. We use NO_2 concentration (surface or column) as an indicator of VOC-limited conditions for NO_x oxidation because Ω_{HCHO} is generally not observable from space in winter. Surface indicators are 24-h averages, while columns are sampled at 9-10 local time (LT) for NH_3 to emulate IASI and at 13-14 LT for NO_2 to emulate OMI. Averaging kernels are applied to the model NO_2 vertical profiles following Cooper et al. (2020) to emulate tropospheric NO_2 columns from version 4 of the NASA OMI NO_2 level 2 product (OMNO2) (Lamsal et al., 2021). We restrict our attention to grid cells with $\Omega_{NO2} > 2.5\times10^{15}$ molec cm^{-2} to remove remote regions (as shown by the satellite observations in Figure 3b) where diagnosing sensitivity to local emissions would be inappropriate.

Results in Figure 2 show that the indicators are successful at diagnosing the dominant pNO_3^- sensitivities to precursor emissions. Black dashed lines delineate the transitions between sensitivity regimes. The slanted lines are derived from reduced-major-axis (RMA) linear regressions for grid cells with sensitivity ratios $0.95 < S_i/S_j < 1.05$. Sensitivities S_{NH3} and S_{NOx} can approach unity within the corresponding regimes. S_{VOC} can reach 0.5 in the VOC-sensitive regime.

Examining first the surface indicators, we find that NH_3-sensitive conditions are defined by $NH_3/HNO_3 < 4$ mol mol^{-1} at low NO_2, with the threshold increasing at higher NO_2. The threshold is larger than the value of 1 for the R ratio in Section 2. This is expected because the gas-phase

HNO_3 concentration can be extremely low in winter, so that competing deposition between gas-phase HNO_3 and pNO_3^- increases sensitivity to NH_3 even when $R > 1$ (Zhai et al., 2021). Outside of the NH_3-sensitive regime, whether NO_x or VOCs is the controlling precursor is well delineated by NO_2 levels. For $NO_2 < 12$ ppb the sensitivity is mostly to NO_x emissions (NO_x-limited regime) but it decreases as NO_2 increases and VOCs then become more important. For $NO_2 > 12$ ppb the sensitivity is mostly to VOCs (strongly VOC-limited regime). NH_3 sensitivity can also be dominant under these conditions because the conversion efficiency of NO_x to HNO_3 is low. The sensitivity regimes separated by the black dashed lines in Figure 2a are thus diagnosed from the gas-phase NH_3/HNO_3 and NO_2 surface indicator concentrations as

$$\text{NH}_3\text{-sensitive:} \begin{cases} \dfrac{\text{NH}_3}{\text{HNO}_3} < 4 & (\text{NO}_2 < 1.3 \text{ ppb}) \\ \log\dfrac{\text{NH}_3}{\text{HNO}_3} < 0.49 + 1.02 \times \log\text{NO}_2 & (\text{NO}_2 > 1.3 \text{ ppb}) \end{cases}, \quad (3a),$$

$$\text{NO}_x\text{-sensitive:} \begin{cases} \dfrac{\text{NH}_3}{\text{HNO}_3} > 4 & (\text{NO}_2 < 1.3 \text{ ppb}) \\ \log\dfrac{\text{NH}_3}{\text{HNO}_3} > 0.49 + 1.02 \times \log\text{NO}_2 & (1.3 \text{ ppb} < \text{NO}_2 < 12 \text{ ppb}) \end{cases}, \quad (3b),$$

$$\text{VOC-sensitive:} \quad \log\frac{\text{NH}_3}{\text{HNO}_3} > 0.49 + 1.02 \times \log\text{NO}_2 \quad (\text{NO}_2 > 12 \text{ ppb}), \quad (3c).$$

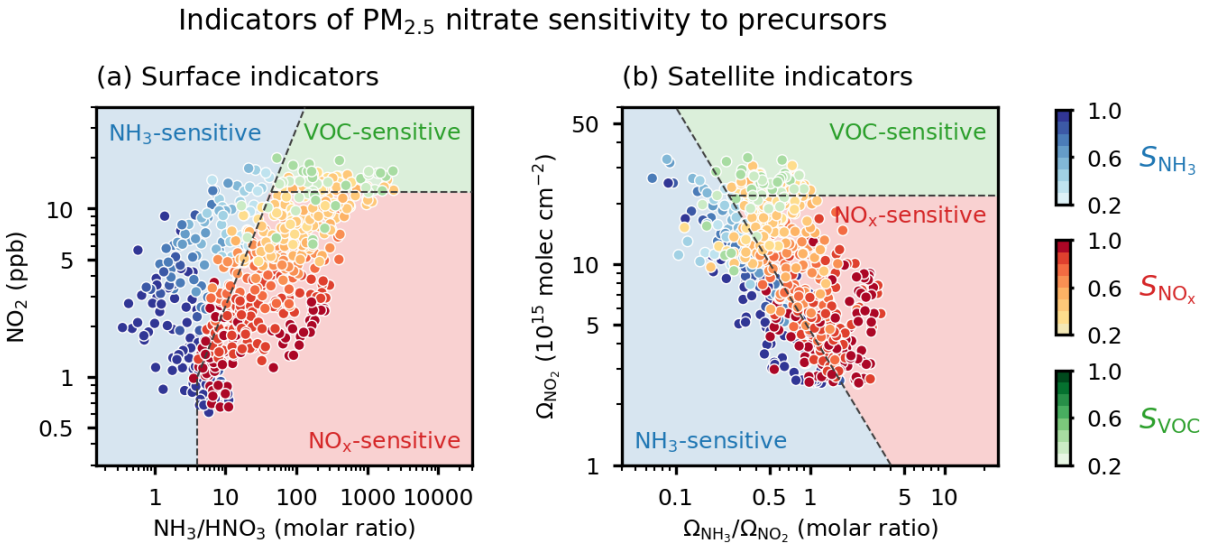

Figure 2. Regimes for the sensitivity of surface pNO_3^- concentrations to NH_3, NO_x, and VOC emissions. Results show the dominant sensitivities $S_i = \Delta\log[pNO_3^-]/\Delta E_i$ for monthly mean concentrations in January 2017 in individual 0.5°×0.625° GEOS-Chem model grid cells in East Asia (domain of Figure 1(a)). A sensitivity $S_i = 1$ indicates proportional response of the pNO_3^- concentration to change in the precursor emission E_i. The dominant sensitivities are plotted in a state space of indicators of the sensitivity regime as observable from surface or satellite measurements. Surface indicators (panel (a)) are the gas-phase NH_3/HNO_3 molar ratio and the NO_2 concentration. Satellite indicators (panel (b)) are the $\Omega_{NH3}/\Omega_{NO2}$ column ratio and the Ω_{NO2}

column. Ω_{NH3} is sampled at 9-10 local time (LT) to emulate the IASI instrument, and Ω_{NO2} is sampled at 13-14 LT to emulate the OMI instrument. Dashed lines separate the different regimes as diagnosed by S_i. The slanted lines are derived from reduced-major-axis (RMA) linear regression for grid cells with sensitivity ratios $0.95 < S_i/S_j < 1.05$. The corresponding equations are given in the text. Ocean and remote grid cells with $\Omega_{NO2} < 2.5\times10^{15}$ molec cm^{-2} (see Figure 3b) are excluded from the plot.

Figure 2b shows that the satellite indicators are similarly effective for diagnosing sensitivity regimes. For a given $\Omega_{NH3}/\Omega_{NO2}$ ratio, higher Ω_{NO2} levels indicate a lower efficiency in converting NO_2 to HNO_3, so that NH_3 is more likely to be in excess. This explains why the threshold $\Omega_{NH3}/\Omega_{NO2}$ ratio for transition from NH_3-sensitive to NO_x-sensitive conditions decreases with increasing Ω_{NO2}, while by contrast the threshold NH_3/HNO_3 ratio in surface observations increases with increasing NO_2. We also see from Figure 2 that Ω_{NO2} can serve as a good satellite indicator for the onset of VOC-sensitive conditions. The sensitivity regimes separated by the black dashed lines in Figure 2b are thus diagnosed from the Ω_{NH3} and Ω_{NO2} columns as

$$\text{NH}_3\text{-sensitive:} \quad \log\frac{\Omega_{NH_3}}{\Omega_{NO_2}} < 14.09 - 0.90 \times \log\Omega_{NO_2} \quad , \qquad (4a),$$

$$\text{NO}_x\text{-sensitive:} \quad \log\frac{\Omega_{NH_3}}{\Omega_{NO_2}} > 14.09 - 0.90 \times \log\Omega_{NO_2} \quad (\Omega_{NO_2} < 2 \times 10^{16} \text{ molec cm}^{-2}), \qquad (4b),$$

$$\text{VOC-sensitive:} \quad \log\frac{\Omega_{NH_3}}{\Omega_{NO_2}} > 14.09 - 0.90 \times \log\Omega_{NO_2} \quad (\Omega_{NO_2} > 2 \times 10^{16} \text{ molec cm}^{-2}), \qquad (4c).$$

4. Application to satellite observations

We now illustrate the application of the method to satellite observations of Ω_{NH3} from IASI and Ω_{NO2} from OMI, using equation (4) to diagnose the sensitivity regimes in the observations. The IASI instrument measures Ω_{NH3} by observing the infrared radiation emitted by the Earth's surface and the atmosphere. It provides global coverage twice a day, at 9:30 local solar time (LT) and 21:30 LT, with a nadir pixel resolution of 12×12 km^2 (Van Damme et al., 2014). The OMI instrument measures Ω_{NO2} by observing solar backscatter, providing daily global coverage at 13:30 LT with a nadir pixel resolution of 13×24 km^2. Here, we use version 3 of the reanalyzed level 2 product of NH_3 columns (ANNI-NH_3-v3R) (Van Damme et al., 2021) and version 4 of the NASA OMI NO_2 level 2 product (OMNO2) (Lamsal et al., 2021) during the winter (DJF) of 2017. Both products have been extensively validated including for IASI v3 (Guo et al., 2021; Vohra et al., 2021; Wang et al., 2022; R. Wang et al., 2023) and OMNO2 version 4 (Lamsal et al., 2021). Both datasets have been used effectively in previous studies for hotspot detection (Mebust et al., 2011; Clarisse et al., 2019) and emission tracking (Shah et al., 2020; Chen et al., 2021; Evangeliou et al., 2021; Marais et al., 2021; Cooper et al., 2022; Luo et al., 2022).

We only use morning overpasses (9:30 LST) for Ω_{NH3} to minimize the time separation with OMI afternoon observations. We filter the IASI Ω_{NH3} data to remove pixels with cloud fraction >0.1. For OMI Ω_{NO2} data, we filter out pixels with cloud fraction >0.3, surface reflectivity >0.3, solar zenith angle >75°, viewing zenith angle >65°, and those affected by the so-called row anomaly.

To reduce noise, both datasets are gridded and averaged to obtain wintertime mean columns at 0.5°×0.625° resolution, and grid cells with fewer than 30 successful retrievals for either Ω_{NH3} or Ω_{NO2} are excluded. Additional filtering is applied to the gridded wintertime means to remove negative values.

Figures 3a and 3b show the IASI Ω_{NH3} and OMI Ω_{NO2} during the winter of 2017. IASI observes high NH_3 in the East China Plain where it originates from livestock waste, fertilizer use, and vehicles (Zhang et al., 2018). OMI observes high NO_2 in the densely populated East China Plain and the Seoul metropolitan area (SMA) in South Korea. These satellite observations of Ω_{NH3} and Ω_{NO2} are roughly consistent with the GEOS-Chem simulations (Figure S1-S2) but that is not a requirement for application of our method.

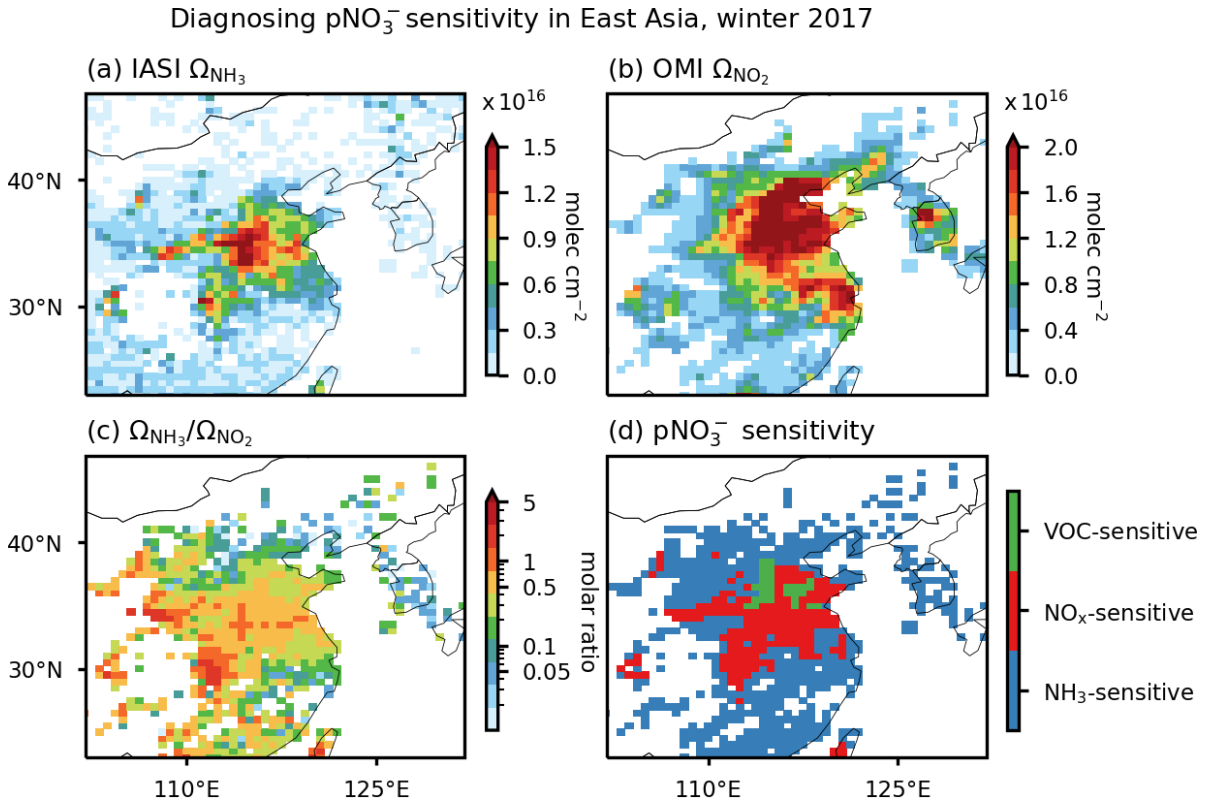

Figure 3. Sensitivity of surface particulate nitrate (pNO_3^-) concentrations in East Asia to precursor emissions as diagnosed from mean satellite observations in winter (DJF) 2016-2017. Panels (a) and (b) show IASI observations of NH_3 columns (Ω_{NH3}) and OMI observations of tropospheric NO_2 columns (Ω_{NO2}), filtered as described in the text. Panel (c) shows the molar $\Omega_{NH3}/\Omega_{NO2}$ ratio computed from the seasonal mean columns. Panel (d) presents the dominant sensitivity regimes of pNO_3^- diagnosed from the satellite observations using equation (4). White areas indicate either lack of data or remote areas ($\Omega_{NO2} < 2.5\times10^{15}$ molec cm^{-2}).

Figure 3d shows the dominant local surface pNO_3^- sensitivities to precursor emissions determined from the observed $\Omega_{NH3}/\Omega_{NO2}$ ratio (Figure 3c) and Ω_{NO2} (Figure 3b) by applying equation (4). We find varying regimes of pNO_3^- sensitivity across China and Korea. VOC-

sensitive conditions are observed in the southern North China Plain (NCP), characterized by a $\Omega_{NH3}/\Omega_{NO2}$ molar ratio exceeding 0.5 and Ω_{NO2} exceeding 2×10^{16} molec cm^{-2}. In this region, pNO_3^- formation is NH_3-saturated, and the most effective approach to decrease pNO_3^- is to control VOC emissions. In other areas of the East China Plain including Henan and Hubei provinces, and in the Fenwei Plain, the satellite observations indicate NO_x-sensitive conditions. In these areas, NH_3 levels are high and NO_x concentrations are not as high as in the southern NCP, so controlling NO_x emissions is the most effective way for decreasing pNO_3^-. NH_3-sensitive conditions are observed in the northern NCP (including Beijing), southern China, and Korea, characterized by relatively low $\Omega_{NH3}/\Omega_{NO2}$ ratios. Our findings are consistent with previous model studies, where wintertime pNO_3^- concentrations are found to be most sensitive to NH_3 and/or VOC controls in the NCP (Fu et al., 2020; Li et al., 2021; Zhai et al., 2021) and to NH_3 controls in the Yangtze River Delta (Li et al., 2021).

Our demonstration of this satellite-based method for diagnosing the sensitivity of pNO_3^- to emissions has focused on wintertime East Asia, where pNO_3^- is particularly high. However, the same method and similar thresholds should be applicable to other polluted regions and seasons. In future work we will extend the application of the method to these other conditions.

In summary, we have shown that NH_3 and NO_2 measurements from space can be used as a NH_3/NO_2 column ratio indicator to diagnose the sensitivity of $PM_{2.5}$ nitrate to emissions in support of pollution management. Our method could be applied to other current satellite instruments including TROPOMI for NO_2 and CrIS for NH_3. Future geostationary satellites including Sentinel-4 and IRS for Europe (Gulde et al., 2017) and GeoXO for the United States (Schmit et al., 2022) will have NO_2 and NH_3 measurements from the same platform. The Nitrosat satellite mission presently under consideration by the European Space Agency will simultaneously observe NH_3 and NO_2 at 500-m resolution, greatly increasing the frequency of clear-sky scenes (Coheur et al., 2021). There is thus considerable potential for application of our method to the next generation of satellite observations.

Acknowledgments

This work was funded by the Harvard–NUIST Joint Laboratory for Air Quality and Climate and the Samsung $PM_{2.5}$ Strategic Research Program. The research in Belgium was supported by the Belgian Science Policy Office (BELSPO, Prodex HIRS and FED-tWIN ARENBERG projects) and the Air Liquide Foundation (TAPIR project). L. Clarisse is Research Associate supported by the Belgian F.R.S.-FNRS.

Data availability

The IASI reanalyzed daily NH_3 data are publicly available from https://iasi.aeris-data.fr/catalog/#masthead. The OMNO2 product, created by the National Aeronautics and Space Administration (NASA), is available for download at https://disc.gsfc.nasa.gov/datasets/OMNO2_003/summary. The $PM_{2.5}$ nitrate observation data that are collected in this study can be accessed via XXX (will be uploaded to Harvard Dataverse (open access)).

References

Alexander, B., Park, R. J., Jacob, D. J., Li, Q. B., Yantosca, R. M., Savarino, J., Lee, C. C. W., and Thiemens, M. H.: Sulfate formation in sea-salt aerosols: Constraints from oxygen isotopes, Journal of Geophysical Research: Atmospheres, 110, https://doi.org/10.1029/2004JD005659, 2005.

Ansari, A. S., and Pandis, S. N.: Response of Inorganic PM to Precursor Concentrations, Environ. Sci. Technol., 32, 2706-2714, 10.1021/es971130j, 1998.

Bressi, M., Cavalli, F., Putaud, J. P., Fröhlich, R., Petit, J. E., Aas, W., Äijälä, M., Alastuey, A., Allan, J. D., Aurela, M., Berico, M., Bougiatioti, A., Bukowiecki, N., Canonaco, F., Crenn, V., Dusanter, S., Ehn, M., Elsasser, M., Flentje, H., Graf, P., Green, D. C., Heikkinen, L., Hermann, H., Holzinger, R., Hueglin, C., Keernik, H., Kiendler-Scharr, A., Kubelová, L., Lunder, C., Maasikmets, M., Makeš, O., Malaguti, A., Mihalopoulos, N., Nicolas, J. B., O'Dowd, C., Ovadnevaite, J., Petralia, E., Poulain, L., Priestman, M., Riffault, V., Ripoll, A., Schlag, P., Schwarz, J., Sciare, J., Slowik, J., Sosedova, Y., Stavroulas, I., Teinemaa, E., Via, M., Vodička, P., Williams, P. I., Wiedensohler, A., Young, D. E., Zhang, S., Favez, O., Minguillón, M. C., and Prevot, A. S. H.: A European aerosol phenomenology - 7: High-time resolution chemical characteristics of submicron particulate matter across Europe, Atmospheric Environment: X, 10, 100108, https://doi.org/10.1016/j.aeaoa.2021.100108, 2021.

Chen, Y., Shen, H., Kaiser, J., Hu, Y., Capps, S. L., Zhao, S., Hakami, A., Shih, J. S., Pavur, G. K., Turner, M. D., Henze, D. K., Resler, J., Nenes, A., Napelenok, S. L., Bash, J. O., Fahey, K. M., Carmichael, G. R., Chai, T., Clarisse, L., Coheur, P. F., Van Damme, M., and Russell, A. G.: High-resolution hybrid inversion of IASI ammonia columns to constrain US ammonia emissions using the CMAQ adjoint model, Atmos. Chem. Phys., 21, 2067-2082, 10.5194/acp-21-2067-2021, 2021.

Chuang, M.-T., Chou, C. C. K., Hsiao, T.-C., Lin, K.-y., Lin, N.-H., Lin, W.-Y., Wang, S.-H., Pani, S. K., and Lee, C.-T.: Analyzing the increasing importance of nitrate in Taiwan from long-term trend of measurements, Atmos. Environ., 267, 118749, https://doi.org/10.1016/j.atmosenv.2021.118749, 2021.

Clarisse, L., Clerbaux, C., Dentener, F., Hurtmans, D., and Coheur, P.-F.: Global ammonia distribution derived from infrared satellite observations, Nat. Geosci., 2, 479-483, 10.1038/ngeo551, 2009.

Clarisse, L., Van Damme, M., Clerbaux, C., and Coheur, P. F.: Tracking down global NH3 point sources with wind-adjusted superresolution, Atmos. Meas. Tech., 12, 5457-5473, 10.5194/amt-12-5457-2019, 2019.

Coheur, P.-F., Levelt, P., Clarisse, L., van Damme, M., Eskes, H., Veefkind, J. P., Clerbaux, C., Dentener, F. J., Erisman, J. W., Schaap, M., Sutton, M. A., and Van Roozendael, M.: Nitrosat, a satellite mission concept for mapping reactive nitrogen at the landscape scale, EGU General Assembly 2021, online, 19–30 Apr 2021, 2021.

Cooper, M. J., Martin, R. V., Henze, D. K., and Jones, D. B. A.: Effects of a priori profile shape assumptions on comparisons between satellite NO2 columns and model simulations, Atmos. Chem. Phys., 20, 7231-7241, 10.5194/acp-20-7231-2020, 2020.

Cooper, M. J., Martin, R. V., Hammer, M. S., Levelt, P. F., Veefkind, P., Lamsal, L. N., Krotkov, N. A., Brook, J. R., and McLinden, C. A.: Global fine-scale changes in ambient NO2 during COVID-19 lockdowns, Nature, 601, 380-387, 10.1038/s41586-021-04229-0, 2022.

Dang, R., Jacob, D. J., Shah, V., Eastham, S. D., Fritz, T. M., Mickley, L. J., Liu, T., Wang, Y., and Wang, J.: Background nitrogen dioxide (NO2) over the United States and its implications for satellite observations and trends: effects of nitrate photolysis, aircraft, and open fires, Atmos. Chem. Phys., 23, 6271-6284, 10.5194/acp-23-6271-2023, 2023.

Duncan, B. N., Yoshida, Y., Olson, J. R., Sillman, S., Martin, R. V., Lamsal, L., Hu, Y., Pickering, K. E., Retscher, C., Allen, D. J., and Crawford, J. H.: Application of OMI observations to a space-based indicator of NOx and VOC controls on surface ozone formation, Atmos. Environ., 44, 2213-2223, https://doi.org/10.1016/j.atmosenv.2010.03.010, 2010.

Evangeliou, N., Balkanski, Y., Eckhardt, S., Cozic, A., Van Damme, M., Coheur, P. F., Clarisse, L., Shephard, M. W., Cady-Pereira, K. E., and Hauglustaine, D.: 10-year satellite-constrained fluxes of ammonia improve performance of chemistry transport models, Atmos. Chem. Phys., 21, 4431-4451, 10.5194/acp-21-4431-2021, 2021.

Fairlie, T. D., Jacob, D. J., Dibb, J. E., Alexander, B., Avery, M. A., van Donkelaar, A., and Zhang, L.: Impact of mineral dust on nitrate, sulfate, and ozone in transpacific Asian pollution plumes, Atmos. Chem. Phys., 10, 3999-4012, 10.5194/acp-10-3999-2010, 2010.

Farren, N. J., Davison, J., Rose, R. A., Wagner, R. L., and Carslaw, D. C.: Underestimated Ammonia Emissions from Road Vehicles, Environ. Sci. Technol., 54, 15689-15697, 10.1021/acs.est.0c05839, 2020.

Fountoukis, C., and Nenes, A.: ISORROPIA II: a computationally efficient thermodynamic equilibrium model for K+-Ca2+-Mg2+-Nh(4)(+)-Na+-SO42--NO3--Cl--H2O aerosols, Atmospheric Chemistry and Physics, 7, 4639-4659, 10.5194/acp-7-4639-2007, 2007.

Franchin, A., Fibiger, D. L., Goldberger, L., McDuffie, E. E., Moravek, A., Womack, C. C., Crosman, E. T., Docherty, K. S., Dube, W. P., Hoch, S. W., Lee, B. H., Long, R., Murphy, J. G., Thornton, J. A., Brown, S. S., Baasandorj, M., and Middlebrook, A. M.: Airborne and ground-based observations of ammonium-nitrate-dominated aerosols in a shallow boundary layer during intense winter pollution episodes in northern Utah, Atmos. Chem. Phys., 18, 17259-17276, 10.5194/acp-18-17259-2018, 2018.

Fu, X., Wang, T., Gao, J., Wang, P., Liu, Y. M., Wang, S. X., Zhao, B., and Xue, L. K.: Persistent Heavy Winter Nitrate Pollution Driven by Increased Photochemical Oxidants in Northern China, Environ. Sci. Technol., 54, 3881-3889, 10.1021/acs.est.9b07248, 2020.

Gulde, S., Kolm, M., Smith, D., Maurer, R., Bazalgette Courrèges-Lacoste, G., Sallusti, M., and Bagnasco, G.: Sentinel 4: a geostationary imaging UVN spectrometer for air quality monitoring: status of design, performance and development, International Conference on Space Optics — ICSO 2014, SPIE, 2017.

Guo, H., Otjes, R., Schlag, P., Kiendler-Scharr, A., Nenes, A., and Weber, R. J.: Effectiveness of ammonia reduction on control of fine particle nitrate, Atmos. Chem. Phys., 18, 12241-12256, 10.5194/acp-18-12241-2018, 2018.

Guo, X., Wang, R., Pan, D., Zondlo, M. A., Clarisse, L., Van Damme, M., Whitburn, S., Coheur, P.-F., Clerbaux, C., Franco, B., Golston, L. M., Wendt, L., Sun, K., Tao, L., Miller, D., Mikoviny, T., Müller, M., Wisthaler, A., Tevlin, A. G., Murphy, J. G., Nowak, J. B., Roscioli, J. R., Volkamer, R., Kille, N., Neuman, J. A., Eilerman, S. J., Crawford, J. H., Yacovitch, T. I., Barrick, J. D., and Scarino, A. J.: Validation of IASI Satellite Ammonia Observations at the Pixel Scale Using In Situ Vertical Profiles, Journal of Geophysical Research: Atmospheres, 126, e2020JD033475, https://doi.org/10.1029/2020JD033475, 2021.

Jin, X., Fiore, A., Boersma, K. F., Smedt, I. D., and Valin, L.: Inferring Changes in Summertime Surface Ozone–NOx–VOC Chemistry over U.S. Urban Areas from Two Decades of Satellite and Ground-Based Observations, Environ. Sci. Technol., 54, 6518-6529, 10.1021/acs.est.9b07785, 2020.

Kim, H., Zhang, Q., and Sun, Y.: Measurement report: Characterization of severe spring haze episodes and influences of long-range transport in the Seoul metropolitan area in March 2019, Atmos. Chem. Phys., 20, 11527-11550, 10.5194/acp-20-11527-2020, 2020.

Kim, J., Jeong, U., Ahn, M.-H., Kim, J. H., Park, R. J., Lee, H., Song, C. H., Choi, Y.-S., Lee, K.-H., Yoo, J.-M., Jeong, M.-J., Park, S. K., Lee, K.-M., Song, C.-K., Kim, S.-W., Kim, Y. J., Kim, S.-W., Kim, M., Go, S., Liu, X., Chance, K., Chan Miller, C., Al-Saadi, J., Veihelmann, B., Bhartia, P. K., Torres, O., Abad, G. G., Haffner, D. P., Ko, D. H., Lee, S. H., Woo, J.-H., Chong, H., Park, S. S., Nicks, D., Choi, W. J., Moon, K.-J., Cho, A., Yoon, J., Kim, S.-k., Hong, H., Lee, K., Lee, H., Lee, S., Choi, M., Veefkind, P., Levelt, P. F., Edwards, D. P., Kang, M., Eo, M., Bak, J., Baek, K., Kwon, H.-A., Yang, J., Park, J., Han, K. M., Kim, B.-R., Shin, H.-W., Choi, H., Lee, E., Chong, J., Cha, Y., Koo, J.-H., Irie, H., Hayashida, S., Kasai, Y., Kanaya, Y., Liu, C., Lin, J., Crawford, J. H., Carmichael, G. R., Newchurch, M. J., Lefer, B. L., Herman, J. R., Swap, R. J., Lau, A. K. H., Kurosu, T. P., Jaross, G., Ahlers, B., Dobber, M., McElroy, C. T., and Choi, Y.: New Era of Air Quality Monitoring from Space: Geostationary Environment Monitoring Spectrometer (GEMS), Bull. Amer. Meteorol. Soc., 101, E1-E22, https://doi.org/10.1175/BAMS-D-18-0013.1, 2020.

Kim, Y., Kim, H., Kang, H., de Foy, B., and Zhang, Q.: Impacts of secondary aerosol formation and long range transport on severe haze during the winter of 2017 in the Seoul metropolitan area, Sci. Total Environ., 804, 149984, https://doi.org/10.1016/j.scitotenv.2021.149984, 2022.

Kleinman, L. I.: Low and high NOx tropospheric photochemistry, Journal of Geophysical Research, 99, 16831-16838, 1994.

Lamsal, L. N., Krotkov, N. A., Vasilkov, A., Marchenko, S., Qin, W., Yang, E. S., Fasnacht, Z., Joiner, J., Choi, S., Haffner, D., Swartz, W. H., Fisher, B., and Bucsela, E.: Ozone Monitoring Instrument (OMI) Aura nitrogen dioxide standard product version 4.0 with improved surface and cloud treatments, Atmos. Meas. Tech., 14, 455-479, 10.5194/amt-14-455-2021, 2021.

Leung, D. M., Shi, H., Zhao, B., Wang, J., Ding, E. M., Gu, Y., Zheng, H., Chen, G., Liou, K.-N., Wang, S., Fast, J. D., Zheng, G., Jiang, J., Li, X., and Jiang, J. H.: Wintertime Particulate Matter Decrease Buffered by Unfavorable Chemical Processes Despite Emissions Reductions in China, Geophys. Res. Lett., 47, e2020GL087721, https://doi.org/10.1029/2020GL087721, 2020.

Li, H., Zhang, Q., Zheng, B., Chen, C., Wu, N., Guo, H., Zhang, Y., Zheng, Y., Li, X., and He, K.: Nitrate-driven urban haze pollution during summertime over the North China Plain, Atmos. Chem. Phys., 18, 5293-5306, 10.5194/acp-18-5293-2018, 2018.

Li, H., Cheng, J., Zhang, Q., Zheng, B., Zhang, Y., Zheng, G., and He, K.: Rapid transition in winter aerosol composition in Beijing from 2014 to 2017: response to clean air actions, Atmos. Chem. Phys., 19, 11485-11499, 10.5194/acp-19-11485-2019, 2019.

Li, M., Zhang, Z., Yao, Q., Wang, T., Xie, M., Li, S., Zhuang, B., and Han, Y.: Nonlinear responses of particulate nitrate to NOx emission controls in the megalopolises of China, Atmos. Chem. Phys., 21, 15135-15152, 10.5194/acp-21-15135-2021, 2021.
Luo, G., Yu, F., and Schwab, J.: Revised treatment of wet scavenging processes dramatically improves GEOS-Chem 12.0.0 simulations of surface nitric acid, nitrate, and ammonium over the United States, Geosci. Model Dev., 12, 3439-3447, 10.5194/gmd-12-3439-2019, 2019.
Luo, G., Yu, F., and Moch, J. M.: Further improvement of wet process treatments in GEOS-Chem v12.6.0: impact on global distributions of aerosols and aerosol precursors, Geosci. Model Dev., 13, 2879-2903, 10.5194/gmd-13-2879-2020, 2020.
Luo, Z., Zhang, Y., Chen, W., Van Damme, M., Coheur, P. F., and Clarisse, L.: Estimating global ammonia (NH3) emissions based on IASI observations from 2008 to 2018, Atmos. Chem. Phys. Discuss., 2022, 1-22, 10.5194/acp-2022-216, 2022.
Marais, E. A., Pandey, A. K., Van Damme, M., Clarisse, L., Coheur, P.-F., Shephard, M. W., Cady-Pereira, K. E., Misselbrook, T., Zhu, L., Luo, G., and Yu, F.: UK Ammonia Emissions Estimated With Satellite Observations and GEOS-Chem, Journal of Geophysical Research: Atmospheres, 126, e2021JD035237, https://doi.org/10.1029/2021JD035237, 2021.
Martin, R. V., Chance, K., Jacob, D. J., Kurosu, T. P., Spurr, R. J. D., Bucsela, E., Gleason, J. F., Palmer, P. I., Bey, I., Fiore, A. M., Li, Q., Yantosca, R. M., and Koelemeijer, R. B. A.: An improved retrieval of tropospheric nitrogen dioxide from GOME, Journal of Geophysical Research: Atmospheres, 107, ACH 9-1-ACH 9-21, https://doi.org/10.1029/2001JD001027, 2002.
Martin, R. V., Fiore, A. M., and Van Donkelaar, A.: Space-based diagnosis of surface ozone sensitivity to anthropogenic emissions, Geophys. Res. Lett., 31, https://doi.org/10.1029/2004GL019416, 2004.
McDuffie, E. E., Smith, S. J., O'Rourke, P., Tibrewal, K., Venkataraman, C., Marais, E. A., Zheng, B., Crippa, M., Brauer, M., and Martin, R. V.: A global anthropogenic emission inventory of atmospheric pollutants from sector- and fuel-specific sources (1970–2017): an application of the Community Emissions Data System (CEDS), Earth Syst. Sci. Data, 12, 3413-3442, 10.5194/essd-12-3413-2020, 2020.
Mebust, A. K., Russell, A. R., Hudman, R. C., Valin, L. C., and Cohen, R. C.: Characterization of wildfire NO_x emissions using MODIS fire radiative power and OMI tropospheric NO₂ columns, Atmos. Chem. Phys., 11, 5839-5851, 10.5194/acp-11-5839-2011, 2011.
Nenes, A., Pandis, S. N., Weber, R. J., and Russell, A.: Aerosol pH and liquid water content determine when particulate matter is sensitive to ammonia and nitrate availability, Atmos. Chem. Phys., 20, 3249-3258, 10.5194/acp-20-3249-2020, 2020.
Petetin, H., Sciare, J., Bressi, M., Gros, V., Rosso, A., Sanchez, O., Sarda-Estève, R., Petit, J. E., and Beekmann, M.: Assessing the ammonium nitrate formation regime in the Paris megacity and its representation in the CHIMERE model, Atmos. Chem. Phys., 16, 10419-10440, 10.5194/acp-16-10419-2016, 2016.
Romer Present, P. S., Zare, A., and Cohen, R. C.: The changing role of organic nitrates in the removal and transport of NOx, Atmos. Chem. Phys., 20, 267-279, 10.5194/acp-20-267-2020, 2020.
Schmit, T. J., Li, Z., Gunshor, M. M., Iturbide-Iturbide, F., Yoe, J. G., McCorkel, J., and Heidinger, A.: U.S. Plans for Geostationary Hyperspectral Infrared Sounders, IGARSS 2022 - 2022 IEEE International Geoscience and Remote Sensing Symposium, 2022, 5411-5414,
Shah, V., Jacob, D. J., Li, K., Silvern, R. F., Zhai, S. X., Liu, M. Y., Lin, J. T., and Zhang, Q.: Effect of changing NOx lifetime on the seasonality and long-term trends of satellite-observed tropospheric NO2 columns over China, Atmospheric Chemistry and Physics, 20, 1483-1495, 10.5194/acp-20-1483-2020, 2020.
Shah, V., Jacob, D. J., Dang, R., Lamsal, L. N., Strode, S. A., Steenrod, S. D., Boersma, K. F., Eastham, S. D., Fritz, T. M., Thompson, C., Peischl, J., Bourgeois, I., Pollack, I. B., Nault, B. A., Cohen, R. C., Campuzano-Jost, P., Jimenez, J. L., Andersen, S. T., Carpenter, L. J., Sherwen, T., and Evans, M. J.: Nitrogen oxides in the free troposphere: implications for tropospheric oxidants and the interpretation of satellite NO2 measurements, Atmos. Chem. Phys., 23, 1227-1257, 10.5194/acp-23-1227-2023, 2023.
Shen, L., Jacob, D. J., Zhu, L., Zhang, Q., Zheng, B., Sulprizio, M. P., Li, K., De Smedt, I., González Abad, G., Cao, H., Fu, T.-M., and Liao, H.: The 2005–2016 Trends of Formaldehyde Columns Over China Observed by Satellites: Increasing Anthropogenic Emissions of Volatile Organic Compounds and Decreasing Agricultural Fire Emissions, Geophys. Res. Lett., 46, 4468-4475, https://doi.org/10.1029/2019GL082172, 2019.
Shephard, M. W., and Cady-Pereira, K. E.: Cross-track Infrared Sounder (CrIS) satellite observations of tropospheric ammonia, Atmos. Meas. Tech., 8, 1323-1336, 10.5194/amt-8-1323-2015, 2015.

Sillman, S.: The use of NO y , H2O2, and HNO3 as indicators for ozone-NO x -hydrocarbon sensitivity in urban locations, Journal of Geophysical Research: Atmospheres, 100, 14175-14188, https://doi.org/10.1029/94JD02953, 1995.

Stelson, A. W., and Seinfeld, J. H.: Relative humidity and temperature dependence of the ammonium nitrate dissociation constant, Atmospheric Environment (1967), 16, 983-992, https://doi.org/10.1016/0004-6981(82)90184-6, 1982.

Tian, M., Liu, Y., Yang, F., Zhang, L., Peng, C., Chen, Y., Shi, G., Wang, H., Luo, B., Jiang, C., Li, B., Takeda, N., and Koizumi, K.: Increasing importance of nitrate formation for heavy aerosol pollution in two megacities in Sichuan Basin, southwest China, Environ. Pollut., 250, 898-905, https://doi.org/10.1016/j.envpol.2019.04.098, 2019.

Van Damme, M., Clarisse, L., Heald, C. L., Hurtmans, D., Ngadi, Y., Clerbaux, C., Dolman, A. J., Erisman, J. W., and Coheur, P. F.: Global distributions, time series and error characterization of atmospheric ammonia (NH₃) from IASI satellite observations, Atmos. Chem. Phys., 14, 2905-2922, 10.5194/acp-14-2905-2014, 2014.

Van Damme, M., Clarisse, L., Franco, B., Sutton, M. A., Erisman, J. W., Wichink Kruit, R., van Zanten, M., Whitburn, S., Hadji-Lazaro, J., Hurtmans, D., Clerbaux, C., and Coheur, P.-F.: Global, regional and national trends of atmospheric ammonia derived from a decadal (2008–2018) satellite record, Environ. Res. Lett., 16, 055017, 10.1088/1748-9326/abd5e0, 2021.

van Geffen, J., Boersma, K. F., Eskesl, H., Sneep, M., ter Linden, M., Zara, M., and Veefkind, J. P.: S5P TROPOMI NO2 slant column retrieval: method, stability, uncertainties and comparisons with OMI, Atmos. Meas. Tech., 13, 1315-1335, 10.5194/amt-13-1315-2020, 2020.

Vohra, K., Marais, E. A., Suckra, S., Kramer, L., Bloss, W. J., Sahu, R., Gaur, A., Tripathi, S. N., Van Damme, M., Clarisse, L., and Coheur, P. F.: Long-term trends in air quality in major cities in the UK and India: a view from space, Atmos. Chem. Phys., 21, 6275-6296, 10.5194/acp-21-6275-2021, 2021.

Wang, R., Pan, D., Guo, X., Sun, K., Clarisse, L., Van Damme, M., Coheur, P. F., Clerbaux, C., Puchalski, M., and Zondlo, M. A.: Bridging the spatial gaps of the Ammonia Monitoring Network using satellite ammonia measurements, EGUsphere, 2023, 1-33, 10.5194/egusphere-2023-190, 2023.

Wang, W., Liu, C., Clarisse, L., Van Damme, M., Coheur, P.-F., Xie, Y., Shan, C., Hu, Q., Sun, Y., and Jones, N.: Ground-based measurements of atmospheric NH3 by Fourier transform infrared spectrometry at Hefei and comparisons with IASI data, Atmos. Environ., 287, 119256, https://doi.org/10.1016/j.atmosenv.2022.119256, 2022.

Wang, X., Jacob, D. J., Downs, W., Zhai, S., Zhu, L., Shah, V., Holmes, C. D., Sherwen, T., Alexander, B., Evans, M. J., Eastham, S. D., Neuman, J. A., Veres, P. R., Koenig, T. K., Volkamer, R., Huey, L. G., Bannan, T. J., Percival, C. J., Lee, B. H., and Thornton, J. A.: Global tropospheric halogen (Cl, Br, I) chemistry and its impact on oxidants, Atmos. Chem. Phys., 21, 13973-13996, 10.5194/acp-21-13973-2021, 2021.

Wang, Y., Wen, Y., Zhang, S., Zheng, G., Zheng, H., Chang, X., Huang, C., Wang, S., Wu, Y., and Hao, J.: Vehicular Ammonia Emissions Significantly Contribute to Urban PM2.5 Pollution in Two Chinese Megacities, Environ. Sci. Technol., 57, 2698-2705, 10.1021/acs.est.2c06198, 2023.

Womack, C. C., McDuffie, E. E., Edwards, P. M., Bares, R., de Gouw, J. A., Docherty, K. S., Dubé, W. P., Fibiger, D. L., Franchin, A., Gilman, J. B., Goldberger, L., Lee, B. H., Lin, J. C., Long, R., Middlebrook, A. M., Millet, D. B., Moravek, A., Murphy, J. G., Quinn, P. K., Riedel, T. P., Roberts, J. M., Thornton, J. A., Valin, L. C., Veres, P. R., Whitehill, A. R., Wild, R. J., Warneke, C., Yuan, B., Baasandorj, M., and Brown, S. S.: An Odd Oxygen Framework for Wintertime Ammonium Nitrate Aerosol Pollution in Urban Areas: NOx and VOC Control as Mitigation Strategies, Geophys. Res. Lett., 46, 4971-4979, https://doi.org/10.1029/2019GL082028, 2019.

Xu, Q., Wang, S., Jiang, J., Bhattarai, N., Li, X., Chang, X., Qiu, X., Zheng, M., Hua, Y., and Hao, J.: Nitrate dominates the chemical composition of PM2.5 during haze event in Beijing, China, Sci. Total Environ., 689, 1293-1303, https://doi.org/10.1016/j.scitotenv.2019.06.294, 2019.

Xu, Z., Liu, M., Zhang, M., Song, Y., Wang, S., Zhang, L., Xu, T., Wang, T., Yan, C., Zhou, T., Sun, Y., Pan, Y., Hu, M., Zheng, M., and Zhu, T.: High efficiency of livestock ammonia emission controls in alleviating particulate nitrate during a severe winter haze episode in northern China, Atmos. Chem. Phys., 19, 5605-5613, 10.5194/acp-19-5605-2019, 2019.

Zhai, S., Jacob, D. J., Wang, X., Shen, L., Li, K., Zhang, Y., Gui, K., Zhao, T., and Liao, H.: Fine particulate matter (PM2.5) trends in China, 2013–2018: separating contributions from anthropogenic emissions and meteorology, Atmos. Chem. Phys., 19, 11031-11041, 10.5194/acp-19-11031-2019, 2019.

Zhai, S., Jacob, D. J., Wang, X., Liu, Z., Wen, T., Shah, V., Li, K., Moch, J. M., Bates, K. H., Song, S., Shen, L., Zhang, Y., Luo, G., Yu, F., Sun, Y., Wang, L., Qi, M., Tao, J., Gui, K., Xu, H., Zhang, Q., Zhao, T., Wang, Y., Lee, H. C., Choi, H., and Liao, H.: Control of particulate nitrate air pollution in China, Nat. Geosci., 14, 389-395, 10.1038/s41561-021-00726-z, 2021.

546 Zhai, S., Jacob, D. J., Pendergrass, D. C., Colombi, N. K., Shah, V., Yang, L. H., Zhang, Q., Wang, S., Kim, H.,
547 Sun, Y., Choi, J. S., Park, J. S., Luo, G., Yu, F., Woo, J. H., Kim, Y., Dibb, J. E., Lee, T., Han, J. S., Anderson, B.
548 E., Li, K., and Liao, H.: Coarse particulate matter air quality in East Asia: implications for fine particulate nitrate,
549 Atmos. Chem. Phys., 23, 4271-4281, 10.5194/acp-23-4271-2023, 2023.
550 Zhang, L., Chen, Y., Zhao, Y., Henze, D. K., Zhu, L., Song, Y., Paulot, F., Liu, X., Pan, Y., Lin, Y., and Huang, B.:
551 Agricultural ammonia emissions in China: reconciling bottom-up and top-down estimates, Atmos. Chem. Phys., 18,
552 339-355, 10.5194/acp-18-339-2018, 2018.
553 Zheng, B., Tong, D., Li, M., Liu, F., Hong, C., Geng, G., Li, H., Li, X., Peng, L., Qi, J., Yan, L., Zhang, Y., Zhao,
554 H., Zheng, Y., He, K., and Zhang, Q.: Trends in China's anthropogenic emissions since 2010 as the consequence of
555 clean air actions, Atmos. Chem. Phys. Discuss., 2018, 1-27, 10.5194/acp-2018-374, 2018.
556 Zhou, M., Nie, W., Qiao, L., Huang, D. D., Zhu, S., Lou, S., Wang, H., Wang, Q., Tao, S., Sun, P., Liu, Y., Xu, Z.,
557 An, J., Yan, R., Su, H., Huang, C., Ding, A., and Chen, C.: Elevated Formation of Particulate Nitrate From N2O5
558 Hydrolysis in the Yangtze River Delta Region From 2011 to 2019, Geophys. Res. Lett., 49, e2021GL097393,
559 https://doi.org/10.1029/2021GL097393, 2022.
560 Zhu, L., Jacob, D. J., Mickley, L. J., Marais, E. A., Cohan, D. S., Yoshida, Y., Duncan, B. N., González Abad, G.,
561 and Chance, K. V.: Anthropogenic emissions of highly reactive volatile organic compounds in eastern Texas
562 inferred from oversampling of satellite (OMI) measurements of HCHO columns, Environ. Res. Lett., 9, 114004,
563 10.1088/1748-9326/9/11/114004, 2014.
564 Zhu, L., Jacob, D. J., Keutsch, F. N., Mickley, L. J., Scheffe, R., Strum, M., González Abad, G., Chance, K., Yang,
565 K., Rappenglück, B., Millet, D. B., Baasandorj, M., Jaeglé, L., and Shah, V.: Formaldehyde (HCHO) As a
566 Hazardous Air Pollutant: Mapping Surface Air Concentrations from Satellite and Inferring Cancer Risks in the
567 United States, Environ. Sci. Technol., 51, 5650-5657, 10.1021/acs.est.7b01356, 2017.
568